



HAL
open science

The role of preferential diffusion on the ignition dynamics of lean premixed hydrogen flames

T. Yahou, N. Detomaso, Laurent Selle, Thierry Poinso, J.R. Dawson, Thierry Schuller, D. Laera

► To cite this version:

T. Yahou, N. Detomaso, Laurent Selle, Thierry Poinso, J.R. Dawson, et al.. The role of preferential diffusion on the ignition dynamics of lean premixed hydrogen flames. Proceedings of the Combustion Institute, 2024, 40 (1-4), pp.105612. 10.1016/j.proci.2024.105612 . hal-04663549v1

HAL Id: hal-04663549

<https://hal.science/hal-04663549v1>

Submitted on 28 Jul 2024 (v1), last revised 5 Sep 2024 (v2)

HAL is a multi-disciplinary open access archive for the deposit and dissemination of scientific research documents, whether they are published or not. The documents may come from teaching and research institutions in France or abroad, or from public or private research centers.

L'archive ouverte pluridisciplinaire **HAL**, est destinée au dépôt et à la diffusion de documents scientifiques de niveau recherche, publiés ou non, émanant des établissements d'enseignement et de recherche français ou étrangers, des laboratoires publics ou privés.

The role of preferential diffusion on the ignition dynamics of lean premixed hydrogen flames

T. Yahou^{a,b,*}, N. Detomaso^c, L. Selle^b, T. Poinso^b, J.R. Dawson^a
T. Schuller^{b,e}, D. Laera^d

^aDepartment of Energy and Process Engineering, Norwegian University of Science and Technology, Trondheim, Norway

^bInstitut de Mécanique des Fluides de Toulouse, IMFT, Université de Toulouse, CNRS, Toulouse, France

^cCERFACS, 42 avenue Gaspard Coriolis, 31057 Toulouse, France

^dDepartment of Mechanics, Mathematics and Management, Polytechnic University of Bari, Via Orabona, 70125 Italy

^eInstitut Universitaire de France (IUF)

Abstract

High-fidelity Large-Eddy Simulations (LES) are used to study the ignition dynamics of two fuel/air mixtures with distinct Lewis numbers Le , unveiling the impact of preferential diffusion during flame expansion including its stabilization above the burner. The simulations cover a CH_4 /air mixture with a unity Lewis number $Le \approx 1$ and a lean H_2 /air mixture with a sub-unity Lewis number $Le \approx 0.34$. Both mixtures are injected at a fixed bulk flow velocity of $U_b = 5 \text{ m.s}^{-1}$, with the equivalence ratio adjusted to match the laminar burning velocity $S_L^0 = 0.25 \text{ m.s}^{-1}$. LES results, including non-reacting flow velocity fields and ignition dynamics, are validated against a large experimental dataset encompassing non-reacting PIV, pressure overshoot, and flame visualization via OH-PLIF. This validation process significantly bolsters confidence in the chosen numerical approach. To elucidate the influence of preferential diffusion on flame propagation during the ignition process, the absolute flame speed is analyzed from kernel initiation, through complete consumption of the fresh gases to flame stabilization. It is found that despite having a lower thermal expansion ratio (ρ_u/ρ_b), the H_2 /air flame still exhibits an enhanced absolute flame speed compared to the CH_4 /air flame. This results in a similar pressure time-series over the full ignition process. An analysis isolating the effects of thermal expansion ratio and stretch effect reveals that this unexpected observation arises from the interplay between preferential diffusion, particularly evident in sub-unity Le mixtures, and the effects driven by the thermal expansion rate. Finally, the role of preferential diffusion and flame stretch on the local flame burning rate is investigated and it is demonstrated that LES can capture the effects of local enrichment observed in DNS studies.

Keywords: Ignition dynamics; Large-eddy simulation; Hydrogen flame; Lewis number effects, Preferential diffusion effects.

Information for Colloquium Chairs and Cochairs, Editors, and Reviewers

1) Novelty and Significance Statement

The primary novelty of this work lies in its exploration of the impact of preferential diffusion on the ignition dynamics of lean premixed flames. LES conducted across the entire ignition sequence of CH₄/air and H₂/air mixtures, each characterized by distinct Lewis numbers. These simulations aim to complement previous experimental observations, revealing the underlying mechanisms inaccessible through experiments, including thermal expansion, flame stretch, and local enrichment. These findings carry practical implications for the design of next-generation H₂-combustion systems, highlighting the pivotal role of preferential diffusion in H₂ flame ignition. Finally, the study underscores the capability of LES to capture these effects when approached methodically, showcasing its potential in comprehending intricate hydrogen combustion dynamics. This understanding could significantly aid in optimizing the design of H₂-combustion technologies.

2) Author Contributions

- T.Y : Designed research, performed experiments, performed simulations, analyzed data, wrote the paper.
- N.D : Designed research, performed simulations, analyzed data, reviewed the paper.
- L.S : Reviewed simulation, reviewed data
- T.P : Reviewed data, reviewed the paper.
- J.R.D: Designed research, reviewed the data, reviewed the paper.
- T.S : Designed research, analyzed data, reviewed the data, reviewed the paper.
- D.L : Designed research, analyzed data, reviewed data, reviewed the paper.

3) Authors' Preference and Justification for Mode of Presentation at the Symposium

The authors prefer **OPP** presentation at the Symposium, for the following reasons:

- As combustion decarbonization, especially with the use of hydrogen, takes center stage at the conference, an oral presentation could initiate engaging discussions among the audience, potentially benefiting the hydrogen community.
- Considering the transient nature of ignition, an oral presentation better suits our study. This format allows the incorporation of animated videos, which are instrumental in conveying nuances that might not be fully appreciated in a poster session.

1. Introduction

Hydrogen has emerged as a promising alternative to hydrocarbon fuels in gas turbines for propulsion, heat and power [1]. Yet, because of its extremely high reactivity and different combustion properties, widespread adoption of hydrogen (H_2) poses significant challenges in combustor design to ensure stability, operability and compliance with engine safety standards [2]. One of these challenges is the need to achieve secure and dependable ignition process across the widest possible range of operating conditions, while mitigating pressure overshoot and preventing flashback post-ignition [3, 4].

Research into the ignition process has concentrated on unraveling fundamental aspects governing the flame dynamics at different times during the ignition sequence [5]. The ignition sequence is generally considered to occur over several phases, namely: kernel formation, flame propagation and flame stabilization. Studies into kernel development and flame propagation have so far pointed out the pivotal mechanisms that dictate the absolute flame propagation speed S_a of a growing flame [6]. In scenarios involving expanding flames in an initially quiescent flow, such as constant volume experiments [2], S_a scales with the unstretched laminar burning velocity S_l^0 propelled by the dilatation ratio, the ratio of the unburned to burned gas densities, (ρ_u/ρ_b) [7]. Studies on more realistic burners have emphasized the significant impact of flow dynamics, notably the effects of turbulence and shear layers, on the flame motion during ignition [8]. More recently, experimental studies on burner-to-burner flame propagation in annular combustors, have shown that in addition to the convection induced by the flow itself, the predominant driver of flame progression is the turbulent flame speed S_T rather than the laminar burning velocity S_l^0 [6, 9]. These studies found that the light-round time is proportional to $\Xi(\rho_u/\rho_b) S_l^0$, where $\Xi = A_T/A_0$ denotes the wrinkling factor that accounts for turbulence. The strong influence of the dilatation ratio and turbulence was also found in Large-Eddy Simulations (LES) of ignition and light-round with liquid spray flames [10, 11].

Yet, the majority of these studies have predominantly centered around hydrocarbon fuels characterized by a unity Lewis number ($Le \approx 1$) which means that the flame is relatively insensitive to local variations in the stretch rate [12]. However, a feature of lean H_2 flames is its sub-unity Lewis number ($Le \ll 1$) which increases the flame sensitivity to stretch effects, further enhancing S_T [8]. Recent Direct Numerical Simulations (DNS) have quantified these local contributions to S_T by introducing a stretch factor I_0 [13–16]. For most conventional hydrocarbon fuels $I_0 = 1$ is observed, whereas above-unity values up to $I_0 = 4$ can be obtained for lean hydrogen mixtures [15]. These effects were suspected to significantly impact the ignition dynamics in both single-sector [4, 17] and annular premixed combus-

tors [18]. In these studies, S_l^0 was fixed for different CH_4/H_2 blends. Yahou et al. [4, 17] found that despite considerable variation in the volumetric expansion ratio (ρ_u/ρ_b) , all blends resulted in similar ignition pressure overshoot, suggesting uniform flame propagation speeds. Using the light around times to estimate the absolute flame speed S_a for different CH_4/H_2 blends, Kwah et al. [18] surprisingly found that S_a increases with decreasing (ρ_u/ρ_b) and suggested that they may result from preferential diffusion effects.

These studies provided the first insight into the effect of hydrogen on ignition dynamics and showed that hydrogen results in distinctly different behaviors compared with conventional fuels. However, these studies were observational and unable to identify the fundamental mechanisms governing the different phases of the ignition sequence. To overcome these experimental limitations, high-fidelity LES are conducted to identify the underlying mechanisms that drive the ignition process of hydrogen flames.

2. Numerical setup and model

LES of the full ignition sequence are conducted on bluff body stabilized premixed flames as described in [17]. Figure 1(a) displays a schematic of the atmospheric combustion rig along side with the main diagnostics. A perforated plate with 0.17 porosity is positioned at the outlet of the combustion chamber to increase the pressure drop and trigger flashback post-ignition. Further details regarding the burner geometry, the ignition system and measurement methods can be found in [4, 17]. The ignition dynamics is investigated under perfectly premixed conditions with a constant bulk flow velocity and fixed laminar burning velocity. Two conditions are examined, a CH_4 /air mixture at $\phi = 0.78$ and an H_2 /air mixture at $\phi = 0.41$ to match $S_l^0 = 0.25 \text{ m.s}^{-1}$. In both scenarios, the bulk flow velocity is set at $U_b = 5 \text{ m.s}^{-1}$. Table 1 lists key combustion properties of the mixtures calculated at ambient temperature 300 K and 1 bar using complex transport in Cantera noting that the H_2 /air flame has a lower thermal expansion ratio but an order of magnitude larger extinction strain rate.

The computational domain used for LES is shown in Fig. 1(b). The full length of the plenum as well as injection pipes are simulated to capture the flow dynamics after ignition and minimize the impact of the boundary conditions. The full domain including the perforated plate is discretized using an unstructured mesh which is refined until a grid-independent solu-

Table 1: Operating conditions and laminar flame properties. Thermal flame thickness δ_{th} and volumetric expansion ratio $\sigma = T_b/T_u$ and extinction strain rate κ_{ext} computed using 1D Twin-Flame framework from CANTERA.

Flame	ϕ	δ_{th} [mm]	S_l^0 [m.s ⁻¹]	σ	κ_{ext} [s ⁻¹]
CH_4/Air	0.78	0.53	0.25	6.7	900
H_2/Air	0.41	0.66	0.25	4.5	3150

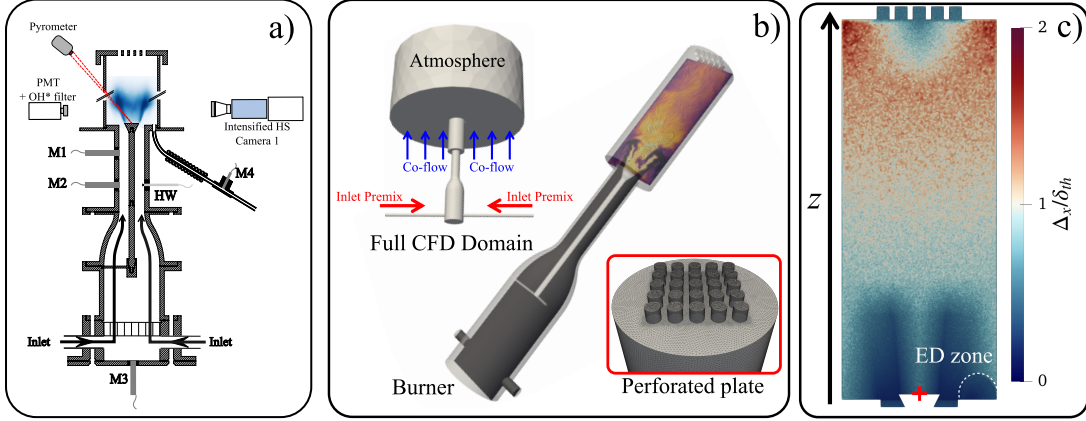


Fig. 1: (a) Schematic of the experimental setup with the main diagnostics. (b) LES computational domain. The full-length plenum and the perforated plate at the chamber outlet are taken into account. (c) Computational grid used inside the combustion chamber. The mesh size Δ_x is normalized by the minimum laminar flame thickness $\delta_{th} = 0.53$ mm of the cases considered in this study (see Table 1). In Fig. (c), the Energy Deposition (ED) zone where $\Delta_x = 60 \mu\text{m}$ is highlighted by the white dashed line. The origin $z = 0$ mm, marked by the red marker, is set at the center of the bluff-body.

tion is obtained. The final mesh counts approximately 92 M tetrahedral elements. The grid has a characteristic size of $\Delta_x = 100 \mu\text{m}$ arranged along the shear layer of the exiting jet. In the spark zone, the mesh is further refined to a characteristic size $\Delta_x = 60 \mu\text{m}$ to ensure a minimum of 8 points within the flame thermal thickness [19] (see Fig. 1(c)). Simulations are performed using the high-fidelity compressible LES solver AVBP (www.cerfacs.fr/avbp7x/). The dynamic thickened flame model DTFLES [20] is used to resolve the flame on the LES grid and the sub-grid turbulent structures are accounted for by the Charlette model [21]. The convective terms are resolved using a third-order accurate Taylor-Galerkin finite-element scheme in both space and time [22]. Sub-grid turbulent scales are modeled using the SIGMA turbulent closure model [23].

Atmospheric pressure is imposed at the outlet of the domain using the Navier–Stokes Characteristic Boundary Conditions (NSCBC) formalism [24]. Inlet mass flow rates are controlled using the generalized non-reflecting boundary conditions NRI-NSCBC [25]. These conditions maintain the specified inlet velocities but permit acoustic fluctuations to leave the domain. The mixture conditions match the experiments ($P = 1$ bar and $T_u = 300$ K). The measured temperature of the bluff body is $T_b = 470$ K in the experiments, while $T_w = 400$ K is imposed for the rest of the chamber walls, including the perforated plate. Thermal losses on the walls are accounted for by applying a heat resistance of $R_w = 2.7 \times 10^{-3} \text{ W.m}^2\text{K}^{-1}$, based on a thermal conductivity of $\lambda = 1.47 \text{ W.m}^{-1}\text{K}^{-1}$ for a 4 mm thick quartz wall.

Ignition is simulated using the energy deposition (ED) model proposed in [26]. A Gaussian-distributed energy source term is applied in both time and space, centered 20 mm away from the burner axis (see Fig. 1(c)) and active between $t = 0$ ms and $t = 0.6$ ms. The total energy deposited matches the exper-

imental spark energy of 36 mJ. Thanks to a high mesh resolution in the ED zone with $\Delta_x = 60 \mu\text{m}$, the flame front is fully resolved to catch kernel formation and ensure that stretch effects on the flame propagation speed are well captured during the earliest stages of ignition sequence when the flame is highly curved. Far from this region, the thickened flame model is smoothly applied reaching a maximum $F = 8$ downstream of the region of interest, where stretch effects are less pronounced [27].

The methane chemical scheme relies on 2-Step BFER global mechanism [28], while hydrogen chemistry is modeled using the semi-detailed San Diego mechanism (9 species and 21 reactions) [29]. To account for preferential diffusion, species transport is modeled using simplified non-unity Lewis number approach for each species. As H_2 and air are perfectly premixed, this approach captures all preferential diffusion effects [16].

3. LES results and validation

3.1. Cold flow velocity fields

The non-reactive velocity fields from LES are initially compared with Particle Image Velocimetry (PIV) measurements obtained before ignition. Time-averages from LES are obtained over an entire flow-through time of the combustion chamber. Azimuthal averaging is conducted to mitigate any spatial dependencies in the flow field. Figure 2 compares experimental (markers) and numerical (solid lines) mean streamwise velocity profiles, along with their corresponding RMS values at various heights $z = 3, 6, 9, 12,$ and 15 mm above the injector. The results show very good agreement between LES and experimental data, accurately capturing both mean velocity \bar{U}_z and RMS fluctuations U_z^{rms} . This underlines the reliability of LES in predicting the shear layers, expansion angles, and turbulence levels. Additionally,

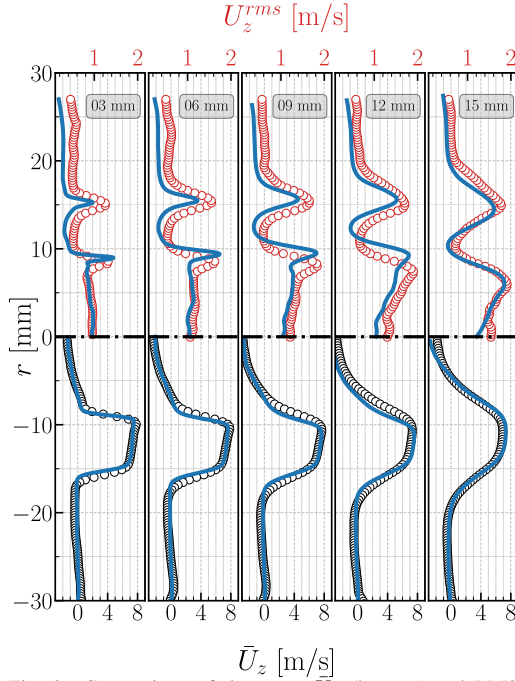


Fig. 2: Comparison of the mean \bar{U}_z (bottom) and RMS U_z^{rms} (top) axial cold flow velocity profiles at five different locations above the injector. Markers denotes PIV data and solid blue line the LES results.

1 the predicted total pressure drop $\Delta P_{LES} = 112$ Pa
 2 across the system corresponding to pressure difference
 3 between the plenum and ambient conditions:
 4 $\Delta P = P_{M3} - P_{atm}$, corresponds to the measured
 5 value of $\Delta P_{exp} = 100$ Pa.

6 3.2. Ignition overpressure and flame dynamics

7 LES and experiments are now compared during the
 8 ignition phase. It is worth noting for the entire ignition
 9 simulation cost is approximately 650 k CPUh for the CH₄ case and about 720 k CPUh for the H₂ case

10 A key indicator of a violent ignition process is the
 11 pressure overshoot relative to the mean value, which
 12 is plotted against time t in Fig. 3 for both CH₄ and
 13 H₂ flames. Pressure time-series are measured at M4
 14 in Fig. 1(a). The average compiled over ten runs,
 15 i.e. ignition sequences performed for each operating
 16 condition is shown by the solid red line with its
 17 'min-max' envelopes (shaded red). The corresponding
 18 pressure signals from LES are plotted in blue. The
 19 time, $t = 0$ ms, marks the appearance of the first
 20 flame kernel. For both operating conditions, the LES
 21 shows excellent agreement with the experiments capturing
 22 both the ignition time and the amplitude of the
 23 pressure impulse, 12 kPa and 14 kPa for CH₄ and
 24 H₂ flames respectively. Despite the transient nature
 25 of the ignition process, the numerical results consistently
 26 fall within the min-max envelope of the experimental
 27 data, the numerical results consistently fall within the
 28 experimental uncertainties with a deviation
 29

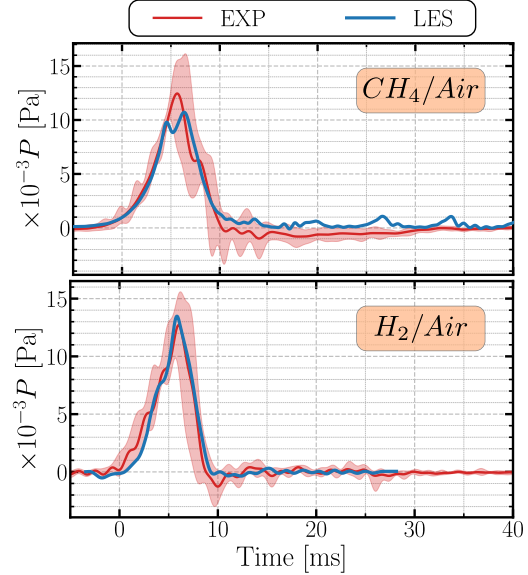


Fig. 3: Time-series of the chamber pressure during ignition. The blue solid line denotes the LES results and red solid line the measurements averaged over 10 runs. The red shaded region corresponds to the 'min-max' envelope.

30 in the amplitude lower than 10%. It is noted that in the
 31 CH₄ case the LES slightly underestimates the peak
 32 amplitude and leads to a larger disparity between the
 33 predicted peak pressures of CH₄ and H₂ flames of ± 4
 34 kPa, compared with ± 2 kPa from the measurements.

35 A qualitative comparison of flame dynamics during
 36 ignition is presented in Fig. 4. It shows OH Planar
 37 Laser Induced Fluorescence OH-PLIF measurements
 38 synchronized with numerical fields of Y_{OH} for H₂ and
 39 Y_{CO_2} for CH₄ flames. The LES successfully predicts
 40 the main features of the flame as it interacts with the
 41 jet shear layer. Due to its lower extinction limit, the
 42 CH₄ flame is quenched near the injector lip in corre-
 43 spondence with the high strained region of the flow
 44 (see Fig. 2) whereas the high extinction strain rate of
 45 the H₂ flame allows it propagate through the main
 46 jet. The simulations also successfully capture the final
 47 stabilization states for each fuel. The CH₄/air flame
 48 is stabilized on the bluff-body whereas the H₂/air
 49 experiences flashback. The good agreement between LES
 50 and experiments demonstrates the robustness of the
 51 selected numerical approach.

52 Figure 5 shows the 3D flame structure represented
 53 by an isosurface of progress variable $c = 1 - (Y_f/Y_f^{in}) = 0.85$ (where Y_f and Y_f^{in} refers to the local and inlet fuel mass fraction, respectively) color-coded by the thickening factor F . Near the injector outlet, where high strain rates occur, both flames feature a restricted thickening factor $F \leq 3$, facilitated by a refined grid in this zone (see Fig. 1(c)). This refinement minimizes the influence of non-resolved sub-grid scales, preserving the Lewis number effects on the flame burning rate [27]. Far from this region,

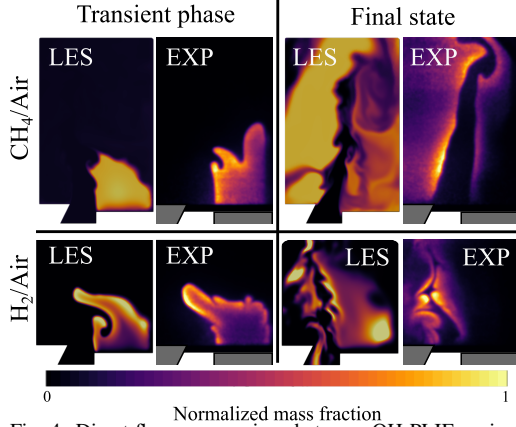


Fig. 4: Direct flame comparison between OH-PLIF against LES Y_{OH} and Y_{CO_2} mass fraction for H_2 and CH_4 flames, respectively. Two instants representing transient flame ignition and final state are shown. Data are normalized by their maximum value for each flame

the flame curvature reduces and larger thickening factors $3 \leq F \leq 8$ are applied. This approach boosts confidence in the numerical simulations by minimizing modeling uncertainties in determining the flame speed, specifically when the flame front is highly curved. It is important to note that the primary aim of this study is to provide insights into the ignition dynamics of lean hydrogen flames. A fundamental investigation of the preferential diffusion effects is beyond the scope of this work and would require highly resolved Direct Numerical Simulations (DNS) [14–16, 30].

4. Flame propagation

4.1. Absolute turbulent flame speed

In the following, the flame dynamics during ignition is scrutinized by focusing on the absolute flame propagation speed S_a which is a significant factor in determining the magnitude of the pressure impulse after ignition [17]. Within this study, S_a is computed

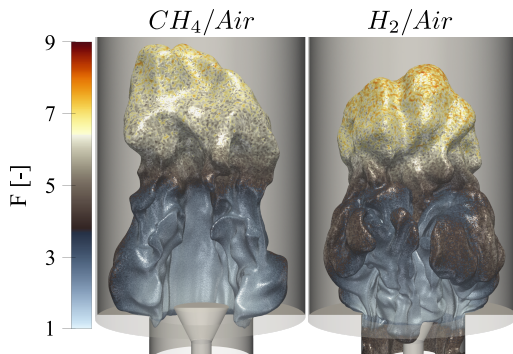


Fig. 5: Variations in the flame thickening factor F for the CH_4/Air (left) and H_2/Air (right) flames.

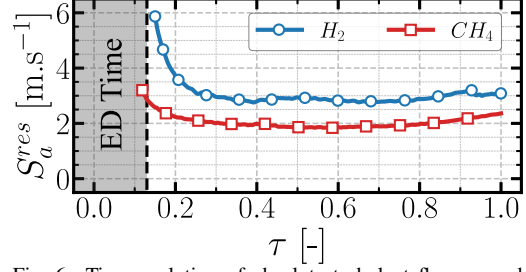


Fig. 6: Time evolution of absolute turbulent flame speed S_a^{res} over the resolved flame surface computed with Eq. (1). The gray shaded region denotes the energy deposition period where the gases are not yet ignited. Time is normalized by t_{HRR} .

during the expansion phase of the initial flame kernel. As illustrated in Fig. 4, the flame takes on an arch-like topology propagating toward the chamber exit. The instant when the flame front reaches the outlet marks the end of the expansion phase which is characterized here by the time-scale when the Heat Release Rate (HRR) reaches its maximum. Throughout this flame expansion phase, an expression for the resolved absolute turbulent flame speed S_a^{res} , i.e. the absolute flame velocity over the resolved flame surface, can be derived by considering the rate of change in the volume of burnt gas as follows [11]:

$$S_a^{res} = \frac{1}{\langle A_T \rangle} \frac{d\langle V_b \rangle}{dt} \quad (1)$$

where $\langle V_b \rangle$ and $\langle A_T \rangle = \int_V |\nabla c| dV$ denote the resolved burnt gas volume and the resolved flame surface area, respectively. Both can be measured in the LES. The normalized time evolution of S_a^{res} for the two fuel mixtures is depicted in Fig. 6 where $\tau = t/t_{HRR}$. The figure shows that following the energy deposition time (gray shaded zone), the initial flame kernel initially propagates at $S_a^{res} = 6.0$ and 3.5 m.s^{-1} for H_2 and CH_4 flames, respectively. The enhancement of S_a^{res} for H_2 is notably stronger than for CH_4 . Shortly after, S_a^{res} quickly reaches a steady value close to 3 m.s^{-1} for H_2 and 2.0 m.s^{-1} for CH_4 throughout the entire expansion phase. Although Table 1 shows that the CH_4/air flame has a greater volumetric expansion ratio, $(\rho_u/\rho_b)S_l^0 = 1.7 \text{ m.s}^{-1}$, than the H_2/air flame, $(\rho_u/\rho_b)S_l^0 = 1.2 \text{ m.s}^{-1}$, the H_2/air flame exhibits a marginally higher propagation speed in Fig. 6. This difference in flame speed likely accounts for the observed difference in the peak pressure impulse observed in Fig. 3. These findings indicate that lean H_2/air mixtures do not follow the conventional expectation of a direct correlation between flame propagation speed and expansion ratio observed in conventional hydrocarbon fuels [6, 9, 31]. The unique combustion properties of lean H_2/air flames, characterized by strong preferential diffusion, makes the flame more susceptible to stretch effects which enhances the burning rate and compensates for the reduced thermal expansion ratio.

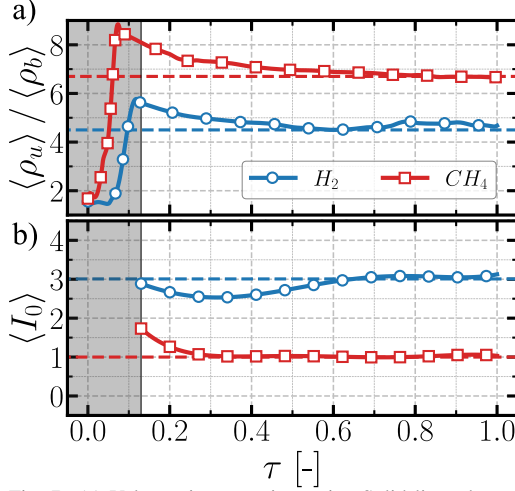


Fig. 7: (a) Volumetric expansion ratio: Solid lines denote LES resolved signal and the dashed lines the values obtained from 1D flame simulation. (b) Stretch factor I_0 computed from Eq. (2).

4.2. Impact of volumetric expansion and stretch

To investigate this latter point, it is instructive to quantify the impact of the volumetric expansion ratio and the stretch effects on the flame propagation speed. The mean stretch factor I_0 averaged over the entire flame surface which accounts for all local variations in the flame structure is evaluated from LES using the relation proposed in [13]:

$$I_0 = \frac{\Omega^*}{S_l^0} \frac{1}{A_T} \quad (2)$$

where

$$\Omega^* = - \frac{\int_V \rho \dot{Y}_f dV}{\rho_u Y_f^{in}} \quad (3)$$

is the normalized total burning rate rate ($\text{m}^3 \cdot \text{s}^{-1}$) over the total volume V , \dot{Y}_f (s^{-1}) is the fuel source term and Y_f^{in} the fuel mass fraction.

The temporal evolution of ρ_u/ρ_b and the stretch factor I_0 during the expansion phase are plotted in Fig. 7(a,b). The results show that soon after ignition both the expansion ratios and stretch factors stabilize, maintaining constant values throughout the entire expansion phase for both fuel mixtures. As anticipated from 1D simulations, a higher thermal expansion ratio is evident for the CH_4/air flame where $\rho_u/\rho_b \simeq 6.7$ compared to $\rho_u/\rho_b \simeq 4.5$ for the H_2/air flame. Interestingly, the opposite trend is observed for the stretch factor I_0 . In the case of CH_4/air mixture with $Le \approx 1$, I_0 stabilizes at a value of 1.0 as expected whereas the lean H_2/air mixture reaches a super-unity value of approximately $I_0 = 3.0$. This discrepancy underscores the pronounced influence of stretch on the propagation speed of the H_2 flame which compensates for any reduction in the thermal expansion ratio compared to the CH_4 flame.

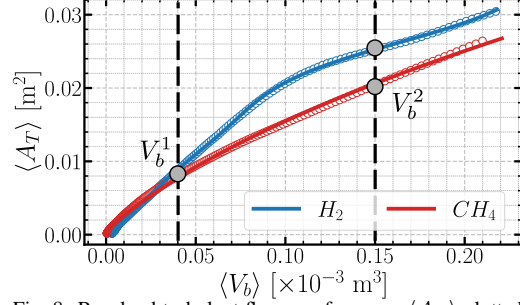


Fig. 8: Resolved turbulent flame surface area $\langle A_T \rangle$ plotted against the burnt gas volume $\langle V_b \rangle$.

In these carefully selected conditions, where the cold flow field and turbulence levels are consistent across both mixtures, the ratio between velocity fluctuations u' and the turbulent integral length scale l_t remains constant in both cases ($u'/l_t = cst$). In addition to the fixed laminar burning velocity S_l^0 , the 1D thermal thickness δ_{th} of both flames differ by less than 8%. Hence, it is reasonable to assume that the flame-turbulence interaction, characterized by the Damköhler number $Da = S_l^0 l_t / u' \delta_{th}$, is comparable for both mixtures. As a consequence, the observed difference in the value of I_0 can therefore be attributed predominantly to thermodynamic effects of lean premixed H_2/air mixtures with $Le \ll 1$.

5. Effect of preferential diffusion

5.1. Flame surface comparison

This section delves into the impact of preferential diffusion by examining the flame dynamics throughout the expansion phase. To illustrate this, Fig. 8 plots the evolution of the turbulent flame surface area $\langle A_T \rangle$ against the burnt gas volume $\langle V_b \rangle$. For small burnt gas volumes, $\langle V_b \rangle \leq V_b^1 = 0.04 \times 10^{-3} \text{ m}^3$, both flames have similar surface areas. However, as the flames grow and produce larger burnt gas volumes $\langle V_b \rangle$, the H_2/air flame exhibits a larger flame surface area for the same burnt gas volume. For example, when $\langle V_b \rangle = V_b^2 = 0.15 \times 10^{-3} \text{ m}^3$ in Fig. 8, the CH_4/air flame has a surface area $\langle A_T \rangle = 200 \text{ cm}^2$ whereas the H_2/air flame shows a total flame surface area $\langle A_T \rangle = 250 \text{ cm}^2$.

The increase in $\langle A_T \rangle$ between H_2 and CH_4 is a direct consequence of preferential diffusion effects which leads to more corrugated flame surface [14]. This is confirmed by comparing the two flames in Fig. 9 which shows snapshots of the 3D isocontour at $c = 0.85$ taken at the burnt gas volume labeled V_b^2 in Fig. 8. It is worth noting that the sub-grid model is the same for both CH_4 and H_2 case, and therefore these thermodynamic effects manifest within the resolved scales of the LES. Models including preferential diffusion effects at the sub-grid scale [32, 33] are not used in the present simulations.

5.2. Flame displacement speed analysis

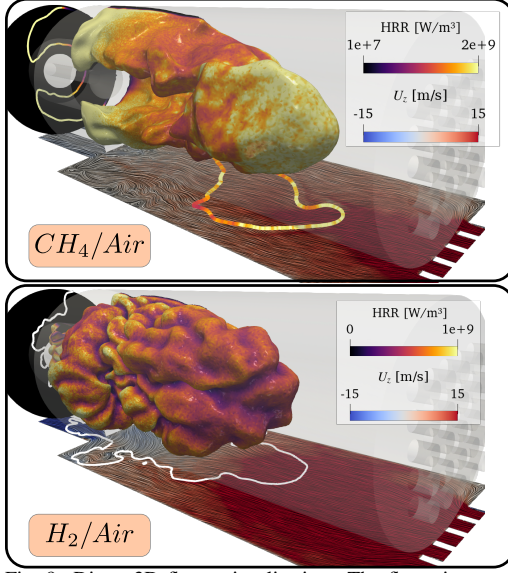


Fig. 9: Direct 3D flame visualisation. The flame is represented by the an iso-surface of progress variable at $c = 0.85$, color-coded by the Heat Release Rate (HRR). The axial velocity in the central plane is also shown.

1 To further elucidate the underlying mechanisms
 2 driving the divergence in the evolution of flame
 3 surface area with respect to burnt gas volume for $V_b >$
 4 V_b^1 in Fig. 8, the density-weighted flame displace-
 5 ment speed $\tilde{S}_d = (\rho/\rho_u) S_d$ is locally analyzed in
 6 Fig. 10, which displays a scatter plot distribution of
 7 \tilde{S}_d , color-coded by the normalized local equivalence
 8 ratio ϕ/ϕ_{in} , with respect to total flame stretch κ [34]:

$$\kappa = -\mathbf{n}\mathbf{n} : \nabla \mathbf{u} + \nabla \cdot \mathbf{u} + S_d (\nabla \cdot \mathbf{n}) \quad (4)$$

9 where \mathbf{n} and \mathbf{u} represent the flame normal and the
 10 flow velocity, respectively. All variables are com-
 11 puted at iso-surface $c = 0.85$ of the progress variable.

12 For the CH_4/air flame, consistent with theoret-
 13 ical expectations, \tilde{S}_d is barely affected by flame
 14 stretch with the scatter distribution close to a constant
 15 value around $\tilde{S}_d \approx 0.3 \text{ m}\cdot\text{s}^{-1}$. This trend is high-
 16 lighted by a linear regression (solid green line), com-
 17 puted by solely considering points exhibiting positive
 18 stretch. As expected for a unity Lewis number com-
 19 bustible mixtures, all flame elements maintain a uni-
 20 form equivalence ratio of $\phi/\phi_{in} = 1$, regardless of
 21 variations in κ .

22 Conversely, for the lean H_2/air flame, \tilde{S}_d increases
 23 with the flame stretch. For the majority of the flame
 24 elements with low stretch values $\kappa \leq 500 \text{ s}^{-1}$, \tilde{S}_d
 25 remains approximately similar to the values observed
 26 for the CH_4/air case between $0.2 \leq \tilde{S}_d \leq 0.5 \text{ m}\cdot\text{s}^{-1}$.
 27 However, for highly stretched flame elements, \tilde{S}_d
 28 exceeds $2.0 \text{ m}\cdot\text{s}^{-1}$ in Fig. 10, emphasizing the substan-
 29 tial impact of preferential diffusion on the flame re-
 30 sponse to stretch, thereby enhancing the flame burn-
 31 ing rate. Moreover, variations in the local equivalence

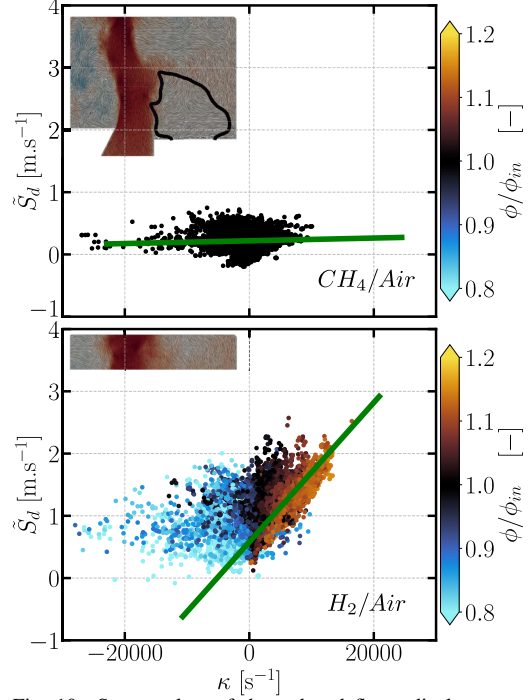


Fig. 10: Scatter plots of the reduced flame displacement speed \tilde{S}_d with respect to the total stretch κ , computed along the iso-surface $c = 0.85$. Data correspond to point V_b^1 in Fig. 8. Scatter plots are colored by local equivalence ratio ϕ/ϕ_{in} .

32 ratio relative to the inlet value value ϕ_{in} are evident.
 33 Flame elements experiencing negative stretch, under
 34 compression, demonstrate local ϕ lower than the inlet
 35 value ($\phi/\phi_{in} < 1$), whereas those subjected to posi-
 36 tive stretch exhibit values exceeding unity ($\phi/\phi_{in} >$
 37 1) increasing the local flame speed. These locally
 38 enriched areas correspond to flame cusps convexly
 39 curved towards the fresh gas, as highlighted from the
 40 slice view in Fig. 10 and observed in previous DNS
 41 studies [14–16].

42 6. Conclusion

43 High-fidelity LES has been used to reveal the im-
 44 pact of preferential diffusion on ignition dynamics
 45 of premixed flames. CH_4 and H_2 fuel/air mixtures
 46 injected with uniform bulk flow velocity have been
 47 considered. The equivalence ratio was varied to
 48 match the laminar unstretched burning velocity for
 49 both mixtures. The numerical approach was validated
 50 against experimental data, including comparison of
 51 the velocity field, flame dynamics and ignition tim-
 52 ing and unsteady pressure are successfully captured
 53 through the entire ignition sequence.

54 LES post-processed results has been used to com-
 55 plement the experiments and identify the mecha-
 56 nisms driving flame propagation during the expansion
 57 phase. Unexpectedly, despite its lower thermal ex-

1 expansion ratio ρ_u/ρ_b , the hydrogen/air flame exhibits
 2 a higher absolute flame speed S_a^{res} compared to the
 3 methane/air mixture. This is attributed to the inter-
 4 play between thermal expansion and stretch effects
 5 evaluated via the stretch factor I_0 . While the CH_4/air
 6 flame has a higher thermal expansion ratio, the H_2/air
 7 flame displays higher I_0 values due to preferential dif-
 8 fusion. Analyzing the local flame dynamics revealed
 9 a uniform density-weighted flame displacement speed
 10 $\tilde{S}_d = (\rho/\rho_b) S_d$ for the CH_4/air flame. However,
 11 for the H_2/air flame, a strong correlation between \tilde{S}_d
 12 and stretch κ emerges indicating that preferential dif-
 13 fusion has a significant impact on the local flame re-
 14 sponse by creating regions of local enrichment along
 15 the flame front that accelerate the flame propagation.

16 Declaration of competing interest

17 The authors declare that they have no known compet-
 18 ing financial interests or personal relationships that
 19 could have influenced the work reported in this paper.

20 Acknowledgments

21 This work was supported by the NCCS Centre
 22 (FME Grant 257579/E20) and received HPC re-
 23 sources from EuroHPC PRACE project No. EHPC-
 24 REG-2023R01-140 (I-MODERN). Special thanks to
 25 Dr. G Staffelbach for assistance with the HPC.

26 References

27 [1] M. Stefanizzi, T. Capurso, G. Filomeno, M. Torresi,
 28 G. Pascazio, Recent Combustion Strategies in Gas Tur-
 29 bines for Propulsion and Power Generation toward a
 30 Zero-Emissions Future: Fuels, Burners, and Combustion
 31 Techniques, *Energies* 14 (20) (2021) 6694.
 32 [2] C. K. Law, G. Jomaas, J. K. Bechtold, Cellular in-
 33 stabilities of expanding hydrogen/propane spherical
 34 flames at elevated pressures: theory and experiment,
 35 *Proc. Combust. Inst.* 30 (1) (2005) 159–167.
 36 [3] M. Fischer, Safety aspects of hydrogen combustion
 37 in hydrogen energy systems, *Int. J. Hydrogen Energy*
 38 11 (9) (1986) 593–601.
 39 [4] T. Yahou, T. Schuller, J. R. Dawson, The Effect of Ig-
 40 nition Procedure on Flashback of Hydrogen-Enriched
 41 Flames, *J. Eng. Gas Turbines Power* 146 (1) (2023).
 42 [5] A. H. Lefebvre, D. R. Ballal, *Gas turbine combustion:*
 43 *alternative fuels and emissions*, CRC press, 2010.
 44 [6] J.-F. Bourgouin, D. Durox, T. Schuller, J. Beaunier,
 45 S. Candel, Ignition dynamics of an annular combustor
 46 equipped with multiple swirling injectors, *Combust.*
 47 *Flame* 160 (8) (2013) 1398–1413.
 48 [7] G. R. Ruetsch, J. E. Broadwell, Effects of confinement
 49 on partially premixed flames, *Annu. Res. Briefs* 1995
 50 (1995).
 51 [8] J. F. Driscoll, Turbulent premixed combustion:
 52 Flamelet structure and its effect on turbulent burning
 53 velocities, *Prog. Energy Combust. Sci.* 34 (1) (2008)
 54 91–134.
 55 [9] R. Ciardiello, P. M. de Oliveira, A. W. Skiba, E. Mas-
 56 torakos, P. M. Allison, Effect of spark location and
 57 laminar flame speed on the ignition transient of a pre-
 58 mixed annular combustor, *Combust. Flame* 221 (2020)
 59 296–310.

[10] K. Töpperwien, S. Puggelli, R. Vicquelin, Analysis of
 flame propagation mechanisms during light-round in
 an annular spray flame combustor: the impact of wall
 heat transfer and two-phase flow, *Combust. Flame* 241
 (2022) 112105.
 [11] S. Puggelli, D. Veynante, R. Vicquelin, Impact of dy-
 namic modelling of the flame subgrid scale wrinkling
 in large-Eddy simulation of light-round in an annular
 combustor, *Combust. Flame* 230 (2021) 111416.
 [12] G. Damköhler, Der einfluss der turbulenz auf die
 flammengeschwindigkeit in gasgemischen, *Zeitschrift
 für Elektrochemie und Angew. Phys. Chemie* 46 (11)
 (1940) 601–626.
 [13] A. Attili, S. Luca, D. Denker, F. Bisetti, H. Pitsch,
 Turbulent flame speed and reaction layer thickening in
 premixed jet flames at constant Karlovitz and increas-
 ing Reynolds numbers, *Proc. Combust. Inst.* 38 (2)
 (2021) 2939–2947.
 [14] L. Berger, A. Attili, H. Pitsch, Synergistic interactions
 of thermodiffusive instabilities and turbulence in lean
 hydrogen flames, *Combust. Flame* 244 (2022) 112254.
 [15] M. Rieth, A. Gruber, F. A. Williams, J. H. Chen, En-
 hanced burning rates in hydrogen-enriched turbulent
 premixed flames by diffusion of molecular and atomic
 hydrogen, *Combust. Flame* 239 (2022) 111740.
 [16] V. Coulon, J. Gaucherand, V. Xing, D. Laera,
 C. Lapeyre, T. Poinso, Direct numerical simulations
 of methane, ammonia-hydrogen and hydrogen turbu-
 lent premixed flames, *Combust. Flame* 256 (2023)
 112933.
 [17] T. Yahou, J. Dawson, T. Schuller, Impact of chamber
 back pressure on the ignition dynamics of hydrogen
 enriched premixed flames, *Proc. Combust. Inst.* 39 (4)
 (2023).
 [18] Y. H. Kwah, S. Wiseman, J. Dawson, The effect of
 methane-ammonia and methane-hydrogen blends on
 ignition and light-around in an annular combustor, *J.
 Eng. Gas Turbines Power* 145 (11) (2023) 1–12.
 [19] B. Rochette, F. Collin-Bastiani, L. Gicquel, O. Ver-
 morel, D. Veynante, T. Poinso, Influence of chemi-
 cal schemes, numerical method and dynamic turbulent
 combustion modeling on LES of premixed turbulent
 flames, *Combust. Flame* 191 (2018) 417–430.
 [20] J.-P. Legier, T. Poinso, D. Veynante, Dynamically
 thickened flame LES model for premixed and non-
 premixed turbulent combustion, in: *Proc. summer
 Progr.*, Vol. 12, Citeseer, 2000, pp. 157–168.
 [21] F. Charlette, C. Meneveau, D. Veynante, A power-law
 flame wrinkling model for LES of premixed turbulent
 combustion Part I: non-dynamic formulation and ini-
 tial tests, *Combust. Flame* 131 (1-2) (2002) 159–180.
 [22] O. Colin, M. Rudgyard, Development of high-order
 Taylor–Galerkin schemes for LES, *J. Comput. Phys.*
 162 (2) (2000) 338–371.
 [23] F. Nicoud, H. B. Toda, O. Cabrit, S. Bose, J. Lee, Us-
 ing singular values to build a subgrid-scale model for
 large eddy simulations, *Phys. fluids* 23 (8) (2011).
 [24] T. J. Poinso, S. K. Lele, Boundary conditions for
 direct simulations of compressible viscous flows, *J.
 Comput. Phys.* 101 (1) (1992) 104–129.
 [25] G. Daviller, G. Oztarlik, T. Poinso, A generalized
 non-reflecting inlet boundary condition for steady and
 forced compressible flows with injection of vortical
 and acoustic waves, *Comput. Fluids* 190 (2019) 503–
 513.
 [26] G. Lacaze, E. Richardson, T. Poinso, Large eddy sim-
 ulation of spark ignition in a turbulent methane jet,

- 1 Combust. Flame 156 (10) (2009) 1993–2009.
- 2 [27] N. Detomaso, J.-J. Hok, O. Dounia, D. Laera,
3 T. Poinso, A generalization of the Thickened Flame
4 model for stretched flames, Combust. Flame 258
5 (2023) 113080.
- 6 [28] B. Franzelli, E. Riber, L. Y. M. Gicquel, T. Poinso,
7 Large eddy simulation of combustion instabilities in a
8 lean partially premixed swirled flame, Combust. Flame
9 159 (2) (2012) 621–637.
- 10 [29] P. Saxena, F. A. Williams, Testing a small detailed
11 chemical-kinetic mechanism for the combustion of hy-
12 drogen and carbon monoxide, Combust. Flame 145 (1-
13 2) (2006) 316–323.
- 14 [30] A. J. Aspden, M. S. Day, J. B. Bell, Characterization of
15 low Lewis number flames, Proc. Combust. Inst. 33 (1)
16 (2011) 1463–1471.
- 17 [31] D. Barré, L. Esclapez, M. Cordier, E. Riber, B. Cuenot,
18 G. Staffelbach, B. Renou, A. Vandel, L. Y. M. Gicquel,
19 G. Cabot, Flame propagation in aeronautical swirled
20 multi-burners: Experimental and numerical investiga-
21 tion, Combust. Flame 161 (9) (2014) 2387–2405.
- 22 [32] T. L. Howarth, A. J. Aspden, An empirical characteris-
23 tic scaling model for freely-propagating lean premixed
24 hydrogen flames, Combust. Flame 237 (2022) 111805.
- 25 [33] A. Aniello, D. Laera, L. Berger, A. Attili, T. Poinso,
26 Introducing thermodiffusive effects in large-eddy sim-
27 ulation of turbulent combustion for lean hydrogen-air
28 flames, CTR, Proc. Summer Progr. 2022 (2022).
- 29 [34] S. M. Candel, T. J. Poinso, Flame stretch and the bal-
30 ance equation for the flame area, Combust. Sci. Technol.
31 70 (1-3) (1990) 1–15.